Case Studies in Construction Materials 15 (2021) e00613

Contents lists available at ScienceDirect

Case Studies in Construction Materials

journal homepage: www.elsevier.com/locate/cscm

Case study

Flexural behavior of high strength concrete deep beams reinforced with GFRP bars

Mona K. Nassif, Abeer M. Erfan, Osama T. Fadel, Taha A. El-sayed *,[1]

Department of Structural Engineering, Shoubra Faculty of Engineering, Benha University, Egypt

ARTICLE INFO

Keywords:
Deep beam
GFRP bars
Flexural
Locally manufactured
HSC
ANSYS 2019-R1

ABSTRACT

This paper presents an experimental and numerical study of the flexural behavior of high concrete deep beams reinforced with locally produced glass fiber reinforced polymers (GFRP) bars using high strength concrete (HSC). Both studies were carried out to study the effect of using (GFRP) bars with different ratios of reinforcement and concrete compressive strengths on the behavior of these beams.

A total of eight beams, measuring 150 mm wide 500 mm depth and 1800 mm length, were cast, and tested up to failure under two-point loading. The main parameters were the types of reinforcement used, whether steel or GFRP bars. Also, concrete compressive strengths of 50 MPa and 60 MPa were used. In addition, different reinforcement ratios of 0.0033 for steel reinforcement and ratios (0.8, 1.0 and 1.2) of the balanced condition were used. The mid-span deflections, failure loads and GFRP reinforcement strains of the examined deep beams were recorded and compared with each other.

The test results revealed that the crack widths and mid-span deflections significantly decreased when using 1.2μb of GFRP reinforcement ratio compared with beams reinforced with steel bars where μb is balanced reinforcement ratio of beam. The decrease in deflection varied between 20%–39.0% for specimens having 50 and 60 MPa respectively, with a significant decrease in the concrete cracks' widths. Also, the ultimate load slightly increased by 2.5 % and 4.0 % as the concrete strengths increased.

A Non-Linear finite element analysis (NLFEA) using ANSYS 2019-R1 was constructed to simulate the flexural behavior of the tested deep beams, in terms of failure load, crack pattern and load deflection behavior. Comparison between the experimental and numerical methods showed good agreement between both results.

1. Introduction

Deep beams have become widely used in high-rise buildings and special structures, and thus have become an important element to be studied. Several researches have been published to study the behavior of reinforced concrete deep beams. [1,2]. Prediction of deep beam behavior using codes is conservative because codes ignore the nonlinear behavior of beams [3,4]. The strength of deep beams depends on the ratio of reinforcement and concrete strength. In some cases, deep beams are exposed to severe environments, and thus

* Corresponding author. Tel.: +20 1008444985.
E-mail address: taha.ibrahim@feng.bu.edu.eg (T.A. El-sayed).
[1] website: http://www.bu.edu.eg/staff/tahaibrahim3

https://doi.org/10.1016/j.cscm.2021.e00613
Received 21 December 2020;
Available online 7 July 2021

Table 1
Concrete Mixes, Materials Weights [20].

Materials	Mix 1 f_{cu} = 50 MP_a	Mix 2 f_{cu} = 60 MP_a
Silica fume	45 Kg/m^3	50 Kg/m^3
Cement	420 Kg/m^3	575 Kg/m^3
Coarse aggregate	1050 Kg/m^3	1100 Kg/m^3
Fine aggregate	680 Kg/m^3	580 Kg/m^3
Water	165 Kg/m^3	138 Kg/m^3
Super-plasticizer	8 L/m^3	18 L/m^3

Table 2
Tensile stresses and Ultimate Strains for used diameters.

Diameter (mm)	Tensile strength (MPa)	Strain mm/mm
8	650	0.0024
10	740	0.0120
12	1075	0.0110

are exposed to corrosion. Corrosion of steel reinforcement leads to cracking of concrete and thus reduces its durability life [5–7]. In the last decades, using FRP bars [21–36] displayed a viable solution to the corrosion problem. These bars are suitable for corrosive environment in several structural applications [2]. Several studies have shown the benefits of using polymers in standard beams [8–10] but there is a shortage for research in studying the behavior of polymers in deep beams. Some research had been done to study the behavior of simply supported deep beams reinforced with FRP bars [11–15]. Nowadays, there is little experimental data conducted for deep beams reinforced with locally manufactured FRP under local conditions and limitations. So, an experimental and numerical study of the flexural behavior of high concrete deep beams reinforced with locally produced glass fiber reinforced polymers (GFRP) bars using high strength concrete (HSC). Both studies were carried out to study the effect of using (GFRP) bars with different ratios of reinforcement varying between 0.8 μb to 1.2 μb. and concrete compressive strengths on the behavior of these beams. Eight beams of 1800 mm length, 500 mm height and 150 mm depth have been studied. These specimens were cast and tested until failure. Nonlinear analysis can take cracking occurring in concrete and yielding in steel into account. Thus, non-linear finite element analysis is necessary to analyze models of concrete structures [16–19] and can provide reliable models of deep beams. Non-Linear Finite Element analysis was done using ANSYS 2019-R1 [38] to verify the obtained experimental results. A comparison was carried out between load-deflection curves, deflections, crack patterns and failure modes obtained from both the experimental and numerical studies. A good agreement between experimental and numerical results was obtained.

1.1. Study objective

The aim of this study to investigate the flexural behavior of the HSC deep beams reinforced with GFRP bars with different reinforcement ratio for different concrete strengths.

2. Experimental program

An experimental study was carried out in the National Building Research Center (NBRC) to study the effect of using GFRP bars in the reinforcement of HSC deep beams. A total of eight beams, measuring 150 mm wide 500 mm depth and 1800 mm length, were cast, and tested up to failure under two-point loading. The main parameters were the types of reinforcement used, whether steel or GFRP bars. Also, concrete compressive strengths of 50 MPa and 60 MPa were used. In addition, different reinforcement ratios of 0.0033 for steel reinforcement and ratios (0.8, 1.0 and 1.2) of the balanced condition were used. The main aim of this research was to study the ultimate load, deflection, strains in concrete and GFRP bars, cracks patterns and its propagation and determine the modes of failure of the beams.

2.1. Experimental program

2.1.1. Concrete mixes

Two concrete mixes were used in the experimental program having compressive strengths of 50 MP_a and 60 MP_a. The materials weights used in these mixes are presented in Table 1.

2.1.2. GFRP glass Fiber reinforcement polymers bars

Due to the limited tensile strength of steel and its ability for corrosion under different parameters; GFRP bars were used instead of steel reinforcement. The tensile strength of GFRP bars for the different bar diameters is given in Table 2.

In order to reduce the cost of the GFRP bars used in the experimental work, it was manufactured locally having deformed similar to those commercially manufactured, the authors produced the GFRP bars employing glass fiber roving and resin. Double plastic molds

Fig. 1. GFRP bars; a) GFRP bars Manufacture, b) GFRP bars diameters.

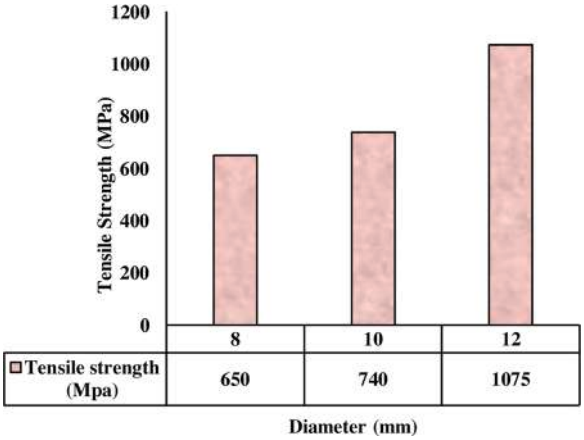

Fig. 2. The Tensile Strength of Examined Diameters.

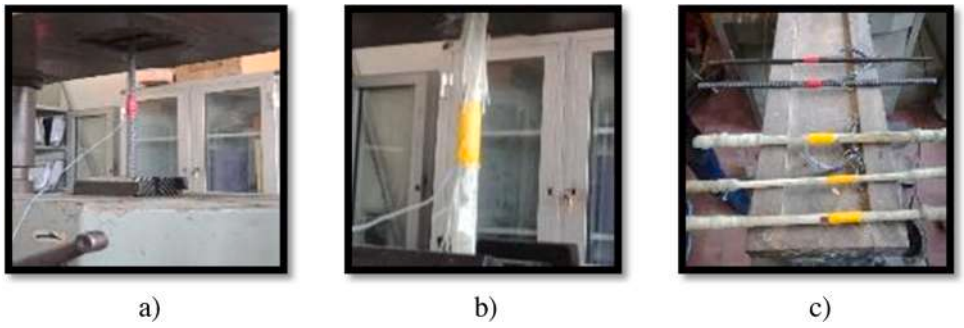

Fig. 3. The Tensile test of reinforcing bars, a) Steel bar; b) GFRP bar; c) All bars' diameters [37].

were constructed to fabricate bars with 8, 10 & 12 mm diameters. The deformed GFRP bars as shown in Fig. 1.

The tensile strength of these bars varied between 650 MP_a, 740 MP_a and 1075 MP_a for diameters 8 mm, 10 mm and 12 mm respectively as shown in Table 2 and Fig. 2. These values were measured due to the pull-out test for these bars carried out in the National Building Research Center as shown in Fig. 3, According to E.S.S, 4756−11, 2012 [37].

Table 3
Specimen's description.

Group	Spec.Id.	Beam Dimension (mm)	RFT. Ratio (μ)	f_{cu} (MPa)	RFT.type	Reinforcement		Shear RFT.	
						Comp.	Ten.	Stirrups	Hzl. steel
I	SP1	150 × 500 × 1800	0.83 μ_{bs}	50	Steel	2Ø10	2Ø12	7Ø8/*m*	2Ø10
	SP3	150 × 500 × 1800	0.80 μ_b	50	GFRP	2Ø10	2Ø10	7Ø8/*m*	2Ø10
	SP4	150 × 500 × 1800	1.00 μ_b	50	GFRP	2Ø10	3Ø10	7Ø8/*m*	2Ø10
	SP5	150 × 500 × 1800	1.20 μ_b	50	GFRP	2Ø10	2Ø12	7Ø8/*m*	2Ø10
II	SP2	150 × 500 × 1800	0.83 μ_{bs}	60	Steel	2Ø10	2Ø12	7Ø8/*m*	2Ø10
	SP6	150 × 500 × 1800	0.80 μ_b	60	GFRP	2Ø10	2Ø10	7Ø8/*m*	2Ø10
	SP7	150 × 500 × 1800	1.00 μ_b	60	GFRP	2Ø10	3Ø10	7Ø8/*m*	2Ø10
	SP8	150 × 500 × 1800	1.20 μ_b	60	GFRP	2Ø10	2Ø12	7Ø8/*m*	2Ø10

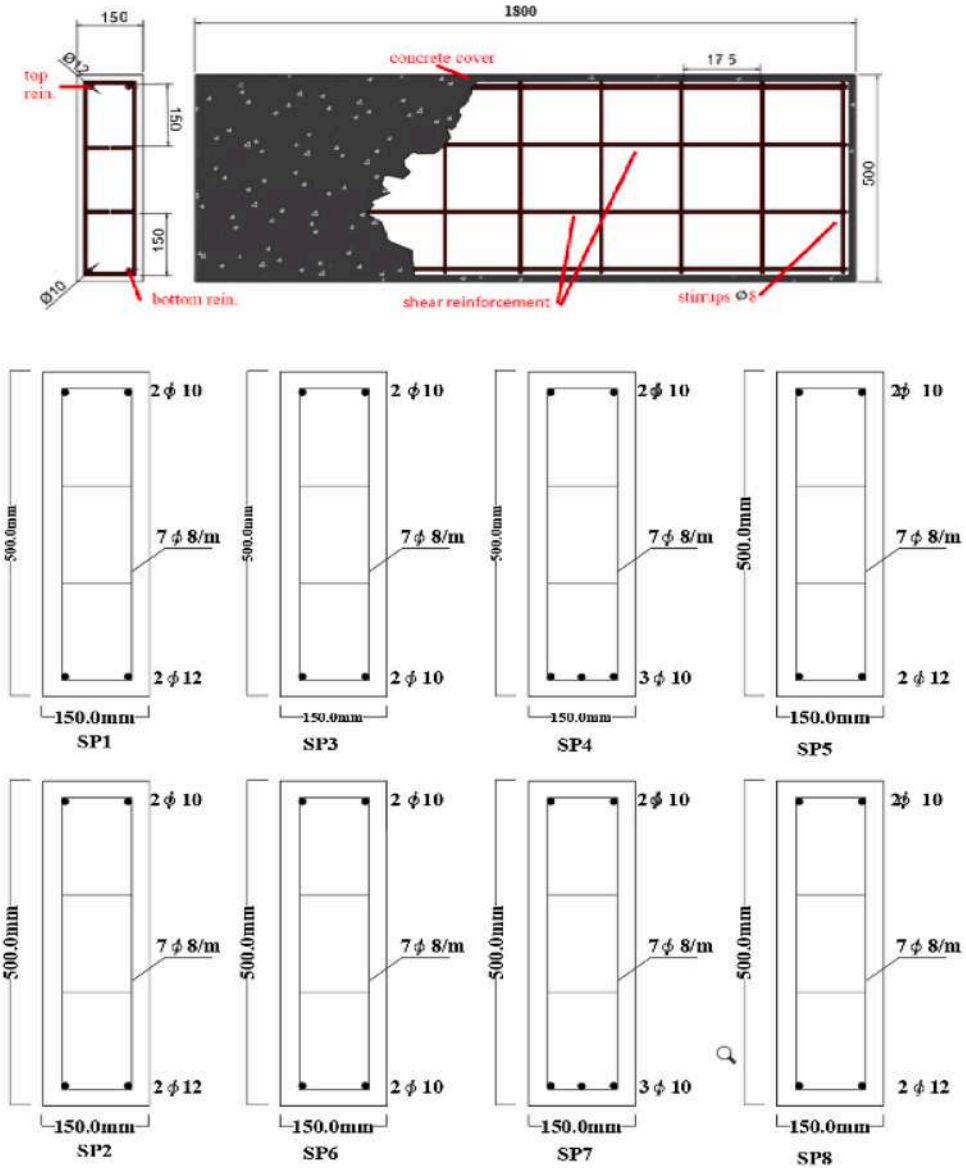

Fig. 4. Deep beams specimens' details.

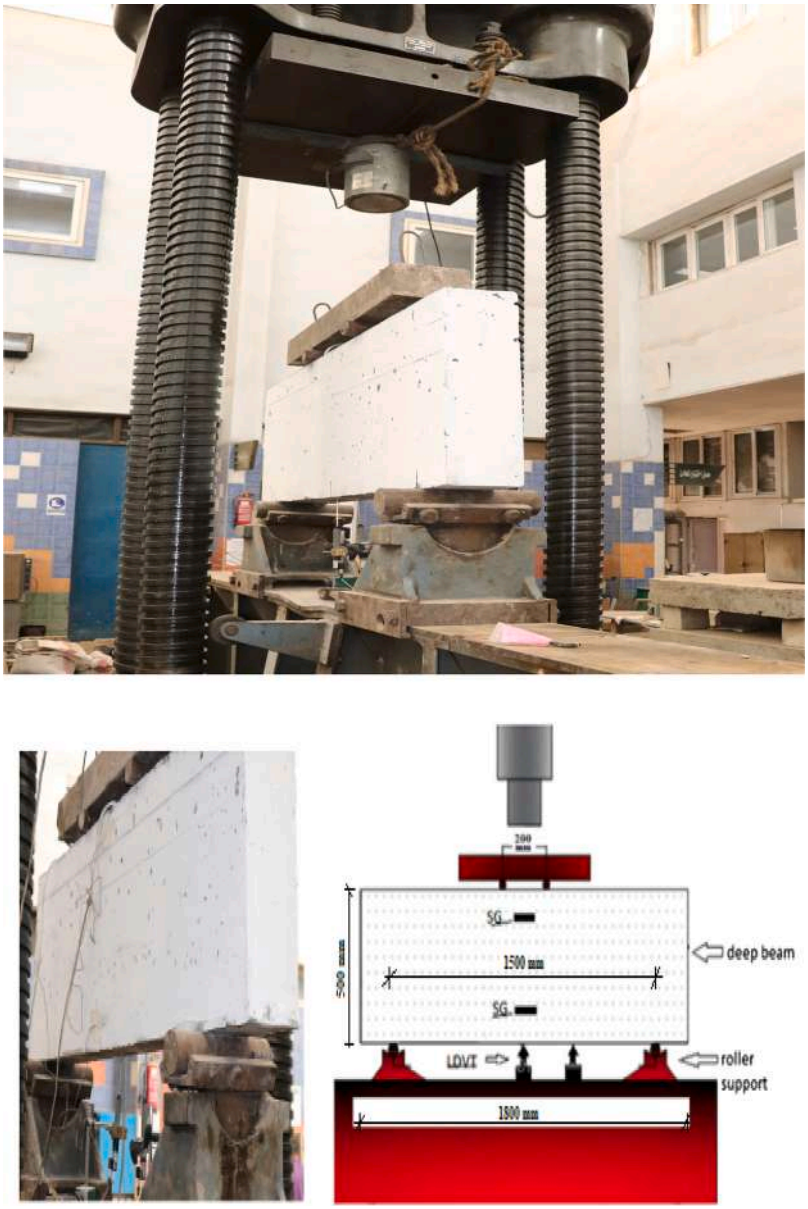

Fig. 5. Deep Beams Test Setup.

2.1.3. Tested deep beams description

The experimental program consists of two groups of concrete deep beams having dimensions of 150 mm, 500 mm height and 1800 mm length. The beams had $\boldsymbol{a/d}$ ratio of 1.33 where $\boldsymbol{a}$ is the distance from the applied load to the center of support and $\boldsymbol{d}$ is the effective depth.

The first group of beams had a concrete compressive strength of 50 MP_a. SP1 is the control specimen in this group which was reinforced using steel bars. SP3, SP4 and SP5 were reinforced using GFRP bars with different ratios of the balanced ratio $\boldsymbol{\mu_b}$ as given in Table 3. The second group had a concrete compressive strength of 60 MPa. For this group, SP2 was the control one which was reinforced using steel bars but SP6, SP8 and SP8 were reinforced using GFRP bars. All details are shown in Table 3 and Fig. 4.

2.2. Test setup

The examined deep beams were tested under a two-point load test having 300 mm between the two points. The test setting was carried out in the National Building Research Center under the universal testing machine having a maximum capacity of 500 tons as shown in Fig. 5. The span length was 1500 mm and the shear span to depth ratio $\boldsymbol{a/d}$ was 1.33. The load was incrementally applied to

Table 4
Experimental failure loads and defections of the tested beams.

Group	Spec. Id.	RFT. Ratio (μ)	f_{cu} (MPa)	Experimental load (kN)		Δ_{uex} (mm)		Ductility% $\frac{\Delta u\ Ult.}{\Delta u\ first}$ x 100%	% of increase Pu	% of decrease In Δu
				First crack load (kN)	Max. load (kN)	Δ_u first crack	Δ_u Ult. crack			
I	SP1	0.83 μ_{bs}	50	170	658.9	0.67	12.24	5.40	———	——
	SP3	0.80 μ_b	50	110	425.5	1.00	5.70	17.50	35.40	53.30
	SP4	1.00 μ_b	50	117	537.5	0.70	6.58	10.60	18.40	46.20
	SP5	1.20 μ_b	50	120	675.3	0.77	9.70	7.90	2.48	20.70
II	SP2	0.83 μ_{bs}	60	175	692.8	0.88	11.88	7.40	——	———
	SP6	0.80 μ_b	60	115	450.7	0.60	9.50	6.30	34.90	20.00
	SP7	1.00 μ_b	60	118	570.1	1.05	9.30	11.20	17.70	21.70
	SP8	1.20 μ_b	60	130	720.4	0.70	7.24	9.67	3.98	39.10

the specimens. Dial gauges with an accuracy of 0.005 mm were placed and LVDTs were used to record the deflection of the beams at mid-span and at 200 mm from supports. The load was increased until failure and the load strains and deflections were recorded.

3. Experimental results and discussion

The experimental results obtained from the experimental testing are presented. These results include the ultimate loads, deflections, load-deflection curves, load-strains for concrete and reinforcement bars, cracks patterns and the obtained modes of failure.

3.1. Experimental ultimate load

The experimental ultimate load was recorded for the first group of deep beams having a compressive strength of concrete 50 MP_a. For the first specimen, SP1, which represents the control specimen, the obtained experimental failure load P_{uexp} was 658.9 kN. For specimens SP3 and SP4 reinforced using GFRP bars with reinforcement ratios equal to and less than $\boldsymbol{\mu_b}$.: the failure load decreased than the control specimen.

For SP5 which was reinforced with 1.2$\boldsymbol{\mu_b}$, the experimental failure load was 675.3 kN with a slight increase of 2.5 % with respect to the control specimen, SP1, as shown in Table 4.

For the specimens of the second group having a concrete compressive strength of 60 MPa; the experimental failure load of the control SP2 was 692.8 kN. For SP6, SP7, reinforced using GFRP bars with reinforcement ratios equal to and less than $\boldsymbol{\mu_b}$; the failure load decreased than the control specimen. For SP8, the failure load was 720.4 kN with a slight increase of 4% with respect to the control specimen, SP2, as shown in Table 4.

Increasing the compressive strength of concrete to 60 MPa in beam SP8, reinforced with 1.2 $\boldsymbol{\mu_b}$, resulted in a significant increase of 10 % in the maximum carrying capacity compared with beam SP1 reinforced with steel and having 50 MPa.

3.2. Crack patterns and modes of failure

3.2.1. Crack patterns and modes of failure of the first group I

The crack pattern of the control beam which had a compressive strength of 50 MPa was featured with cracks propagation in the tension zone. The first flexural crack appeared at a load of 170 kN and shear cracks appeared at a load of 425.0 kN from the support point. The flexure cracks propagated and increased in width until the flexural failure load of 658.9 kN was reached, as shown in Fig. 6. Shear cracks did not reach the point of application of the loads and hence the failure mode was tension failure T.F.

For specimen SP3 which was reinforced using a GFRP reinforcement ratio of 0.8μ_b, the first crack appeared at a load of 110 kN. The flexural cracks propagated and increased in width until rupture of GFRP bars occurred. This rupture was accompanied with excessive flexural cracking and spalling of concrete at the tension zone.

For specimen SP4 which was reinforced using a GFRP reinforcement ratio of μ_b, the first crack appeared at a load of 117.0 kN. Cracks in the compression strut zone started at 330 kN and increased in number and width in this zone, as shown in Fig. 6c. The specimen failed at the GFRP rupture at a load of 537.5 kN. The failure can be considered as a rupture failure combined with strut compression failure.

For specimen SP5 which was reinforced with GFRP reinforcement of 1.2 μ_b, the cracks started at 120 kN. The cracks propagated and increased in number and width until the GFRP rupture in the tension zone accompanied with concrete spalling as shown in Fig. 6d.

3.2.2. Crack patterns and modes of failure of the second group II

The crack pattern of the control beam for this group SP2, which had a compressive strength of concrete of 60 MPa was featured with cracks propagation in the tension zone. The first crack appeared at a load of 175 kN and shear cracks appeared at a load of 680 kN from the support point but did not reach the point of application of loads. The flexural cracks propagated and increased in width till flexural failure took place at a load of 692.8 kN, as shown in Fig. 7. The failure mode was tension failure T.F.

For specimen SP6 which was reinforced using GFRP with a reinforcement ratio of 0.8μ_b, the first crack load appeared at 115 kN. The flexural cracks propagated and increased in width till rupture of GFRP bars occurred. There was an improvement in the crack's

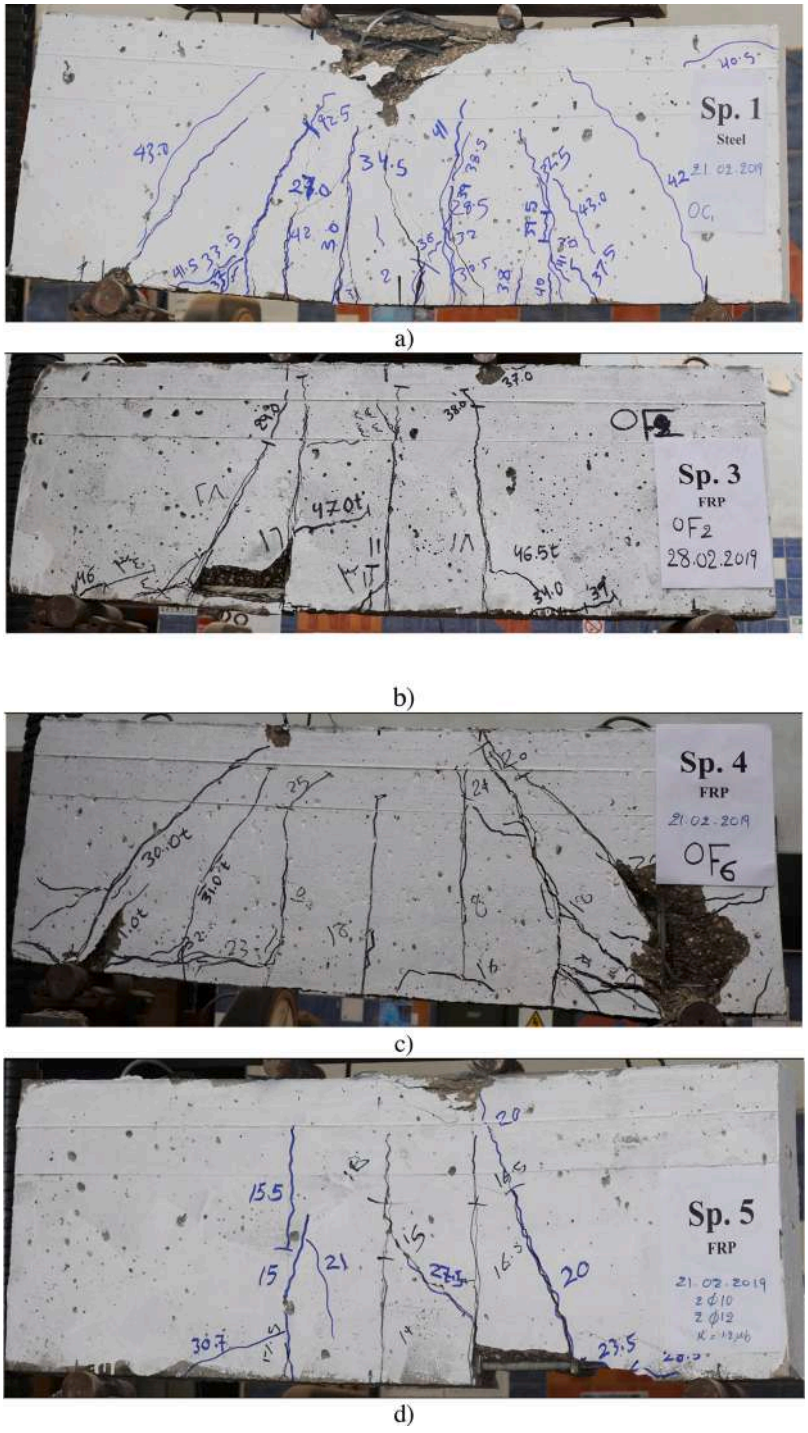

Fig. 6. Cracks Patterns for Group I; a) SP1; b) SP3, c) SP4, d) SP5.

propagation due to the high compressive concrete especially in the strut zone till failure at 450.7 kN.

For specimen SP7 which was reinforced using a reinforcement ratio of $1.0\mu_b$ GFRP bars, the first crack appeared at a load of 118 kN. The cracks increased in number and width especially in the tension zone. There was an improvement in the crack's propagation especially in the strut zone due to the high compressive concrete strength of concrete and GFRP bars rupture occurred at a load of 570.1 kN indicating failure.

For specimen SP8 which was reinforced with a reinforcement of ratio of $1.2\ \mu_b$ GFRP bars, the cracks started at 130 kN. The number

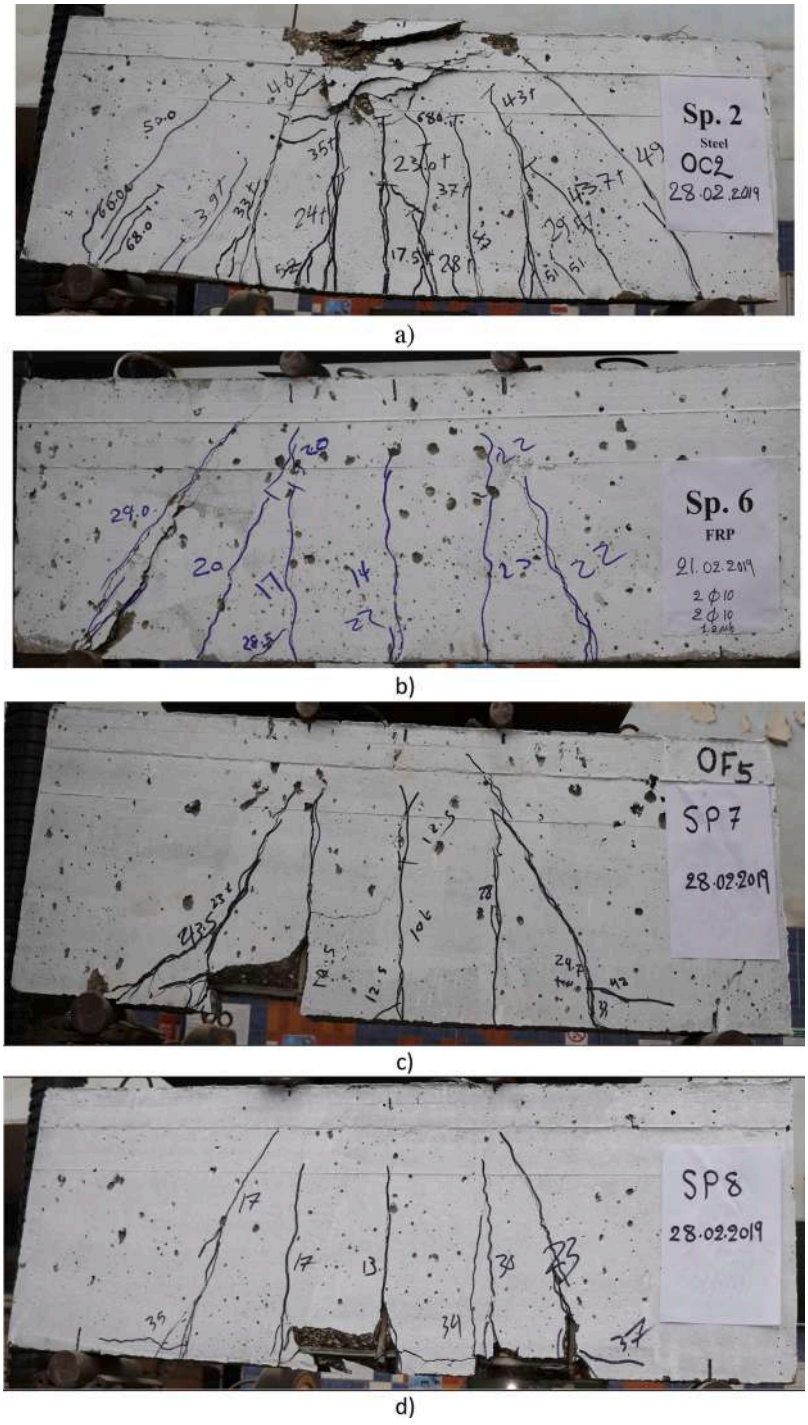

Fig. 7. Cracks Patterns for Group II; a) SP2; b) SP6, c) SP7, d) SP8.

of cracks and propagation decreased with respect to specimen SP5 till GFRP rupture occurred in the tension zone accompanied with concrete spalling as shown in Fig. 7.

3.3. Mid- span load-deflection behavior

Firstly, all beams display linear elastic behavior up to the cracking load when the concrete cracked at the tension face. Then, the beams stiffness, mostly for the GFRP RC beams, was reduced at a faster rate, resulting in a larger deflection. This might be due to low

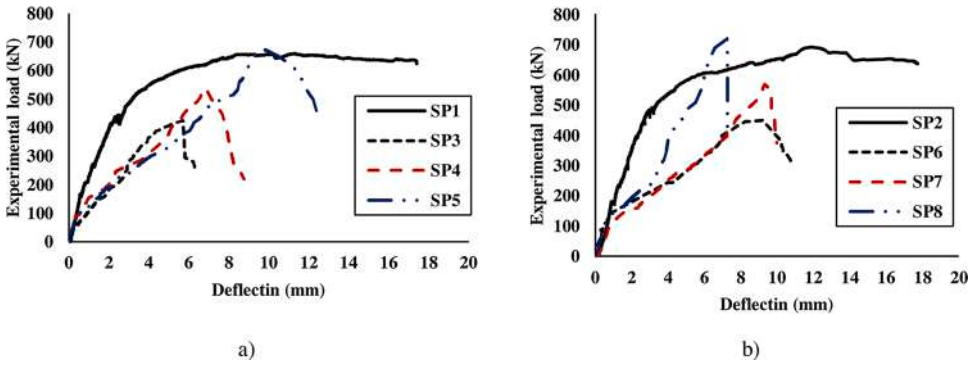

Fig. 8. load deflection curve; a) fcu = 50 MPa, b) fcu = 60 MPa.

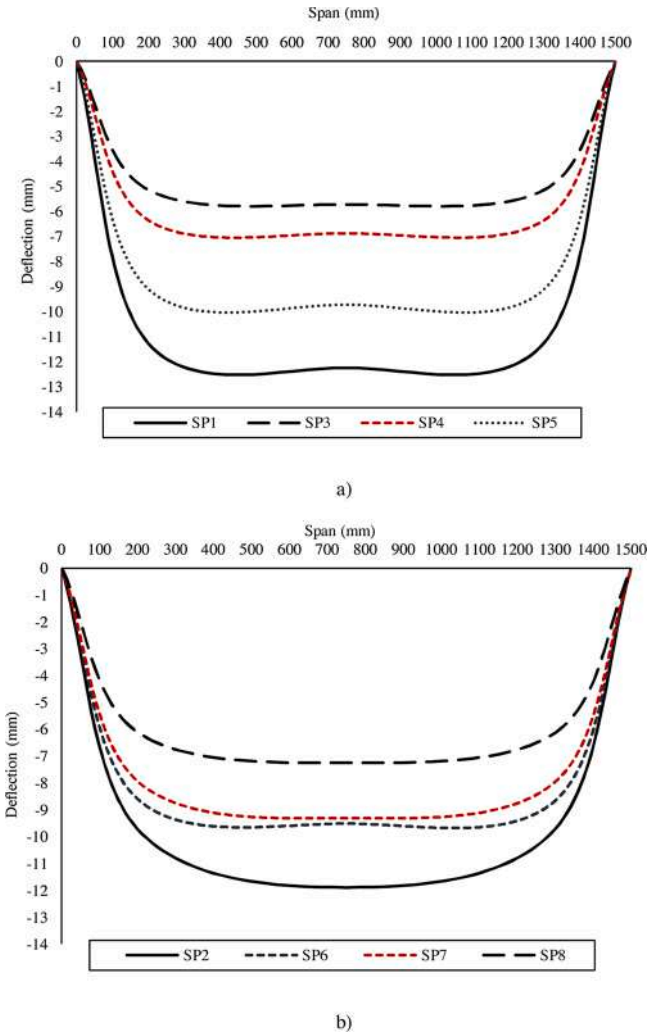

Fig. 9. Relative Distance- Deflection through Span Length; a) fcu = 50 MPa, b) fcu = 60 MPa.

elastic modulus of the GFRP bars compared to reinforcing steel bars. The loads deflection curves for all GFRP beams were bilinear. The first portion of the curve till cracking represents the uncracked behavior of beams. The second portion represents the cracked behavior beams with reduced stiffness. But GFRP beams with 1.2μb reinforcement ratio were confirmed some ductility which could be provided by the concrete throughout the concrete crushing failure mechanism.

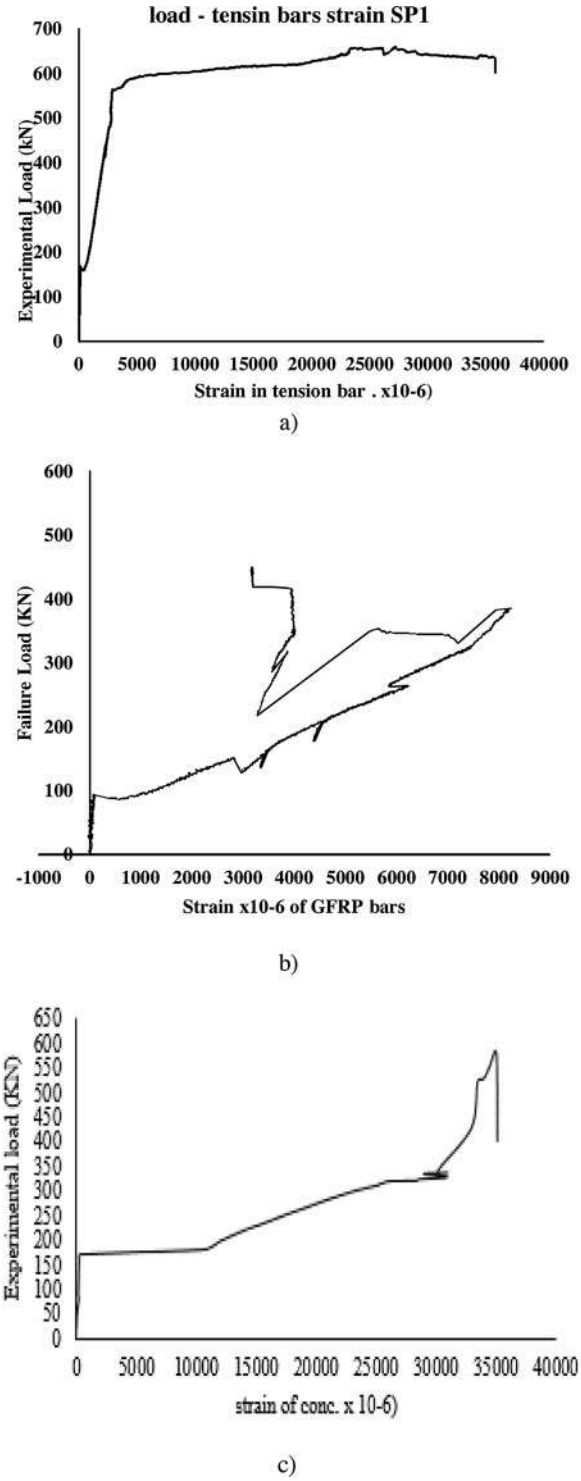

Fig. 10. Strains of Tested Beams a) Failure in Steel bars, b) Rupture failure in GFRP bars, c) Failure in concrete.

Table 4 indicates the obtained deflections for all the tested specimens. For the first group having f_{cu} 50 MP_a, the recorded deflections showed a good enhancement due to using GFRP bars with respect to SP1 reinforced using steel bars.

The deflection of SP1 recorded 12.24 mm at failure load but it recorded 5.70 mm, 6.58 mm, and 9.70 mm for SP3, SP4, and SP5. Thus, for beam SP5, reinforced with $1.2\mu_b$, the deflection decreased by 20 % than beam SP1 reinforced with steel.

For the second group, the deflection recorded values of 11.88 mm, 9.50 mm, 9.30 mm, and 7.24 mm for SP2, SP6, SP7, and SP8,

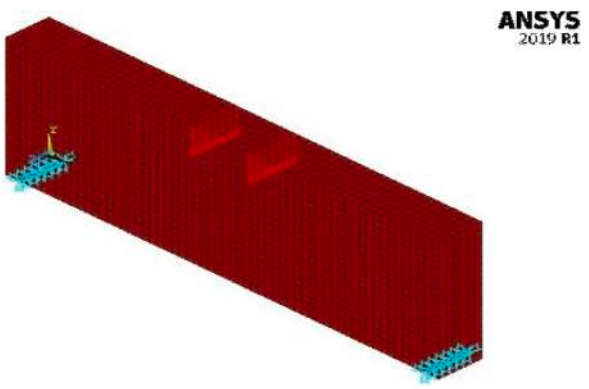

Fig. 11. 3D-Beam Model.

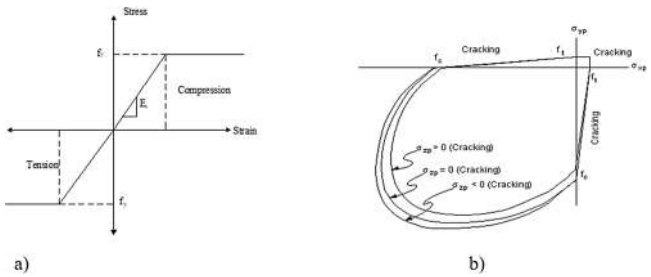

Fig. 12. Material behaviors; a) Link180 Spar Idealized Stress-Strain Relationship of Steel Reinforcement; b) Solid 65 Failure Surface in Principal Stress Space in Biaxial State of Stresses in concrete.

Table 5
FEM material properties.

HSC deep beam (GI)			HSC deep beam (GII)		
Material	Element	Material Properties	Material	Element	Material Properties
HSC (GI)	Solid 65	Elastic modulus of elasticity (E_c=33.234 GPa) Poisson's ratio (PRXY) ($\nu = 0.3$) Compressive strength ($f_{cu} = 50$ MPa) Tensile strength (f_t =5 MPa)	HSC (GII)	Solid 65	Elastic modulus of elasticity (E_c =36.406 GPa) Poisson's ratio (PRXY) ($\nu = 0.3$) Compressive strength ($f_{cu} = 60$ MPa) Tensile strength (f_t =6 MPa)
Reinforcing steel bars (GI)	Link180	Elastic Modulus of elasticity (E_s = 200,000 MPa) Poisson's ratio (PRXY) ($\nu = 0.2$) Yield stress for deformed steel bars (f_y = 400 MPa) Area of steel of φ12 (As = 113 mm2) Area of steel of φ10 (As = 78.5 mm2) Yield stress for stirrups ($f_{yst} = 240$ MPa) Area of steel of φ8 (As = 50.3 mm2)	Reinforcing steel bars (GII)	Link180	Elastic Modulus of elasticity (E_s = 200,000 MPa) Poisson's ratio (PRXY) ($\nu = 0.2$) Yield stress for deformed steel bars (f_y = 400 MPa) Area of steel of φ12 (As = 113 mm2) Area of steel of φ10 (As = 78.5 mm2) Yield stress for stirrups ($f_{yst} = 240$ MPa) Area of steel of φ8 (As = 50.3 mm2)
GFRP bars (GI)	Link180	Elastic Modulus of elasticity (E_f = 42.5 GPa) Tensile strength of φ8 ($f_t = 650$ MPa) Tensile strength of φ10 ($f_t = 740$ MPa) Tensile strength of φ12 ($f_t = 1075$ MPa) Poisson's ratio (PRXY) ($\nu = 0.2$) Area of steel of φ12 (As = 113 mm2) Area of steel of φ10 (As = 78.5 mm2) Area of steel of φ8 (As = 50.3 mm2)	GFRP bars (GII)	Link180	Elastic Modulus of elasticity (E_f = 42.5 GPa) Tensile strength of φ8 ($f_t = 650$ MPa) Tensile strength of φ10 ($f_t = 740$ MPa) Tensile strength of φ12 ($f_t = 1075$ MPa) Poisson's ratio (PRXY) ($\nu = 0.2$) Area of steel of φ12 (As = 113 mm2) Area of steel of φ10 (As = 78.5 mm2) Area of steel of φ8 (As = 50.3 mm2)

respectively. Specimen SP8 showed a significant decrease in the deflection of about 39 %. This indicates the beneficial effect of GFRP bars in significantly decreasing the deflections as shown in Fig. 8.

The recorded deflections in the deep beams' specimens at different distances through the beam spans is indicted in Fig. 9.

Table 6
NLFEA Results.

Group	Spec. Id.	RFT. Ratio (μ)	f_{cu} (MPa)	NLFE failure load (kN)		Δ_{NLFE} (mm)		Ductility% $\frac{\Delta u\ Ult.}{\Delta u\ first}$ x 100%
				First crack load (kN)	Max. load (kN)	Δ_u Ult. crack	Δ_u first crack	
I	SP1	$0.83\mu_{bs}$	50	90.0	560.1	10.4	0.56	5.38
	SP3	$0.80\ \mu_b$	50	90.0	382.9	5.13	0.90	17.50
	SP4	$1.00\ \mu_b$	50	90.0	483.7	5.13	0.63	12.30
	SP5	$1.20\ \mu_b$	50	90.0	587.5	6.16	0.67	10.80
II	SP2	$0.83\mu_{bs}$	60	110.0	609.7	8.40	0.77	9.16
	SP6	$0.80\ \mu_b$	60	110.0	405.6	7.83	0.51	6.50
	SP7	$1.00\ \mu_b$	60	110.0	456.1	7.44	0.84	10.70
	SP8	$1.20\ \mu_b$	60	110.0	657.3	7.0	0.56	8.00

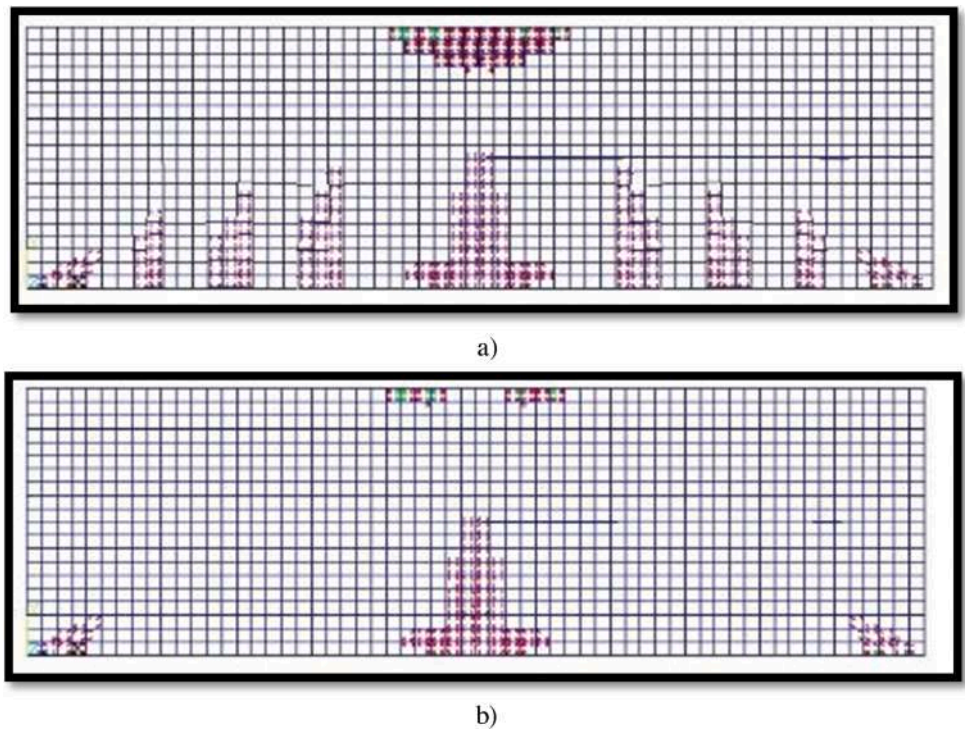

Fig. 13. NLFE Cracks Patterns; a) Beams Reinforced Using Steel Bars; b) Beams Reinforced Using GFRP.

3.4. Strains and ductility of the tested beams

Strain gauges were fixed on each of the concrete in tension and compression zones, on tension-steel bars and on GFRP bars. This was to record the strains of each element and determine its maximum strain value identifying the mode of failure of the deep beams. In the beams reinforced using steel bars, the maximum concrete strain was 0.0035 which exceeded the maximum value causing tension failure.

For specimens SP3 and SP6 reinforced using (2φ10) GFRP bars, the recorded strains for the GFRP bars at failure reached its ultimate value and were equal to 0.012. Thus, rupture of the bars took place, and the failure mode was rupture failure accompanied with concrete spalling as shown in Figs. 8 and 9.

For SP4, the recorded GFRP strain was 0.01 and the recorded concrete strain was 0.005, exceeding the ultimate values. Thus, rupture of the GFRP bars took place accompanied with concrete compression strut failure. However, when the concrete strength was increased to 60 MPa in SP7, the concrete strain recorded a value less than its ultimate value, while GFRP strain reached its ultimate value. Accordingly, rupture of GFRP bars took place while no concrete compression strut failure was recorded.

For specimens SP5 and SP8, the recorded strain in the GFRP bars was 0.0124 and 0.01 respectively causing rupture of the bars accompanied with an increase in the number of the tension concrete cracks. Fig. 10 indicated strains obtained from steel bars, GFRP bars and concrete in tension strain.

For the obtained ductility from the experimental results for the first group of f_{cu} 50 MPa, the ductility percentages were 5.40, 17.5, 10.6 and 7.90 for SP1, SP3, SP4 and SP5, respectively. This shows the effect of using CFRP bars in increasing the duality as in Table 4.

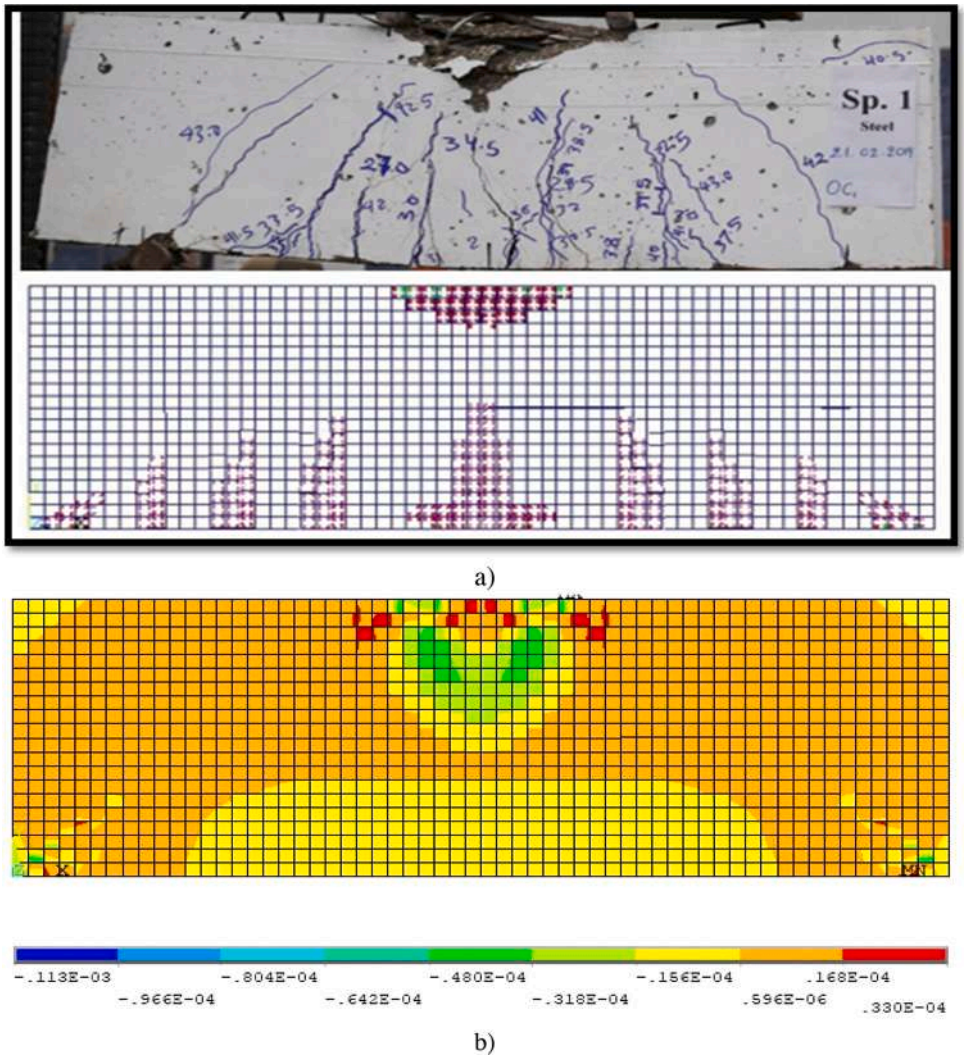

Fig. 14. a) Comparisons between Experimental and NLFE Cracks Patterns for Beams Reinforced Using Steel bars.
b) Strain mapping for Beams Reinforced Using Steel bars.

With the same manner for second group of f_{cu} 60 MPa, the recorded ductility percentages for SP2, SP6, SP7 and SP8 were 7.40, 6.30, 11.2 and 9.67 respectively which showing the enhancement.

4. Non-linear finite element analysis

4.1. Modeling

In the present study, a NLFEA was carried out to investigate the flexural behavior of HSC deep beams reinforced with GFRP bars. The NLFEA program used was ANSYS-2019-R1 [38] software which has several three-dimensional elements in its library as SOLID65 as it is suitable for presentation of compression stress-strain curve for concrete other properties. Link180 element of two nodes was used to model the steel reinforcement and GFRP bars. Each node has three degrees of freedom, translation in X, Y, and Z directions. This indicated in Fig. 11. The investigated behavior includes the crack patterns, the ultimate carrying capacity, and deflections of the examined beams.

4.2. The constitutive model used in FEM

For concrete elements, SOLID65 used in ANSYS program but Link180 was used to represent the elements of steel and GFRP bars. Fig. 12 showed the curves for each element in NLFE program.

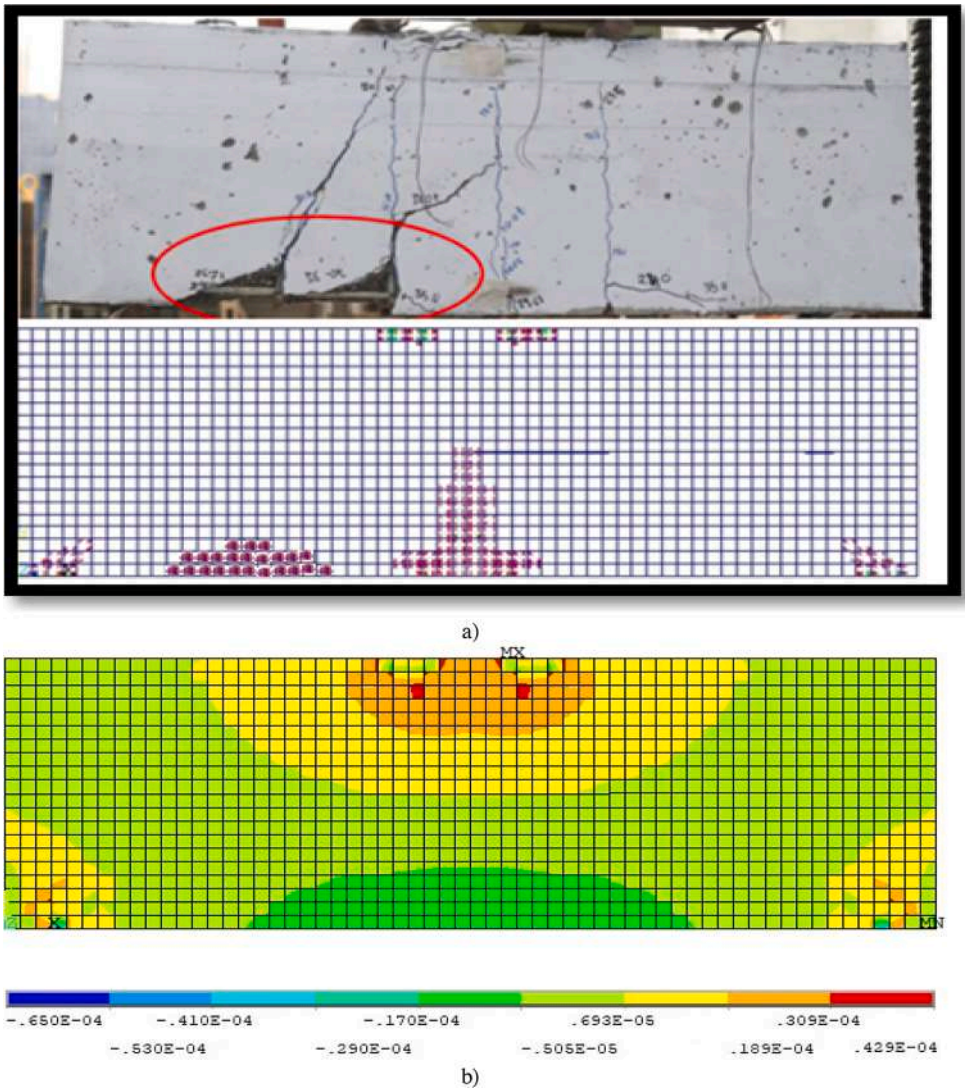

Fig. 15. a) Comparisons between Experimental and NLFE Cracks Patterns for Beams Reinforced Using 1.2 μb GFRP bars.
b) Strain mapping for Beams Reinforced Using 1.2 μb GFRP bars.

4.3. Mesh-sensitivity analysis

To get good results from the Solid65 elements, using a rectangular mesh was recommended. The global mesh of the concrete as in Fig. 11. Maximum meshing dimension for all models is 25 × 25 mm. It is suggested to use a minimum of 4–6 elements per beam thickness. A mesh sensitivity analysis was carried out to control the optimal mesh size. As the finite elements mesh size become smaller, the computational time of the software increases.

4.4. Input parameters for materials

Table 5 showed the needed parameters to assign the models material properties for HSC deep beams, steel bars and GFRP bars.

4.5. NLFE ultimate failure loading

The theoretical ultimate load was recorded for the first group of deep beams with a compressive strength of concrete 50 MPa. For the first specimen, SP1, which represents the control specimen, the obtained theoretical failure load $P_{U\ NLFEA}$ was 560.1 kN. For the specimens reinforced using GFRP bars SP3 and SP4, no increase was obtained in the theoretical failure load. For SP5 which was reinforced using 2Φ12 GFRP bars in tension, the theoretical failure load was 587.5 kN with a slight increase with respect to SP1 as shown in Table 6.

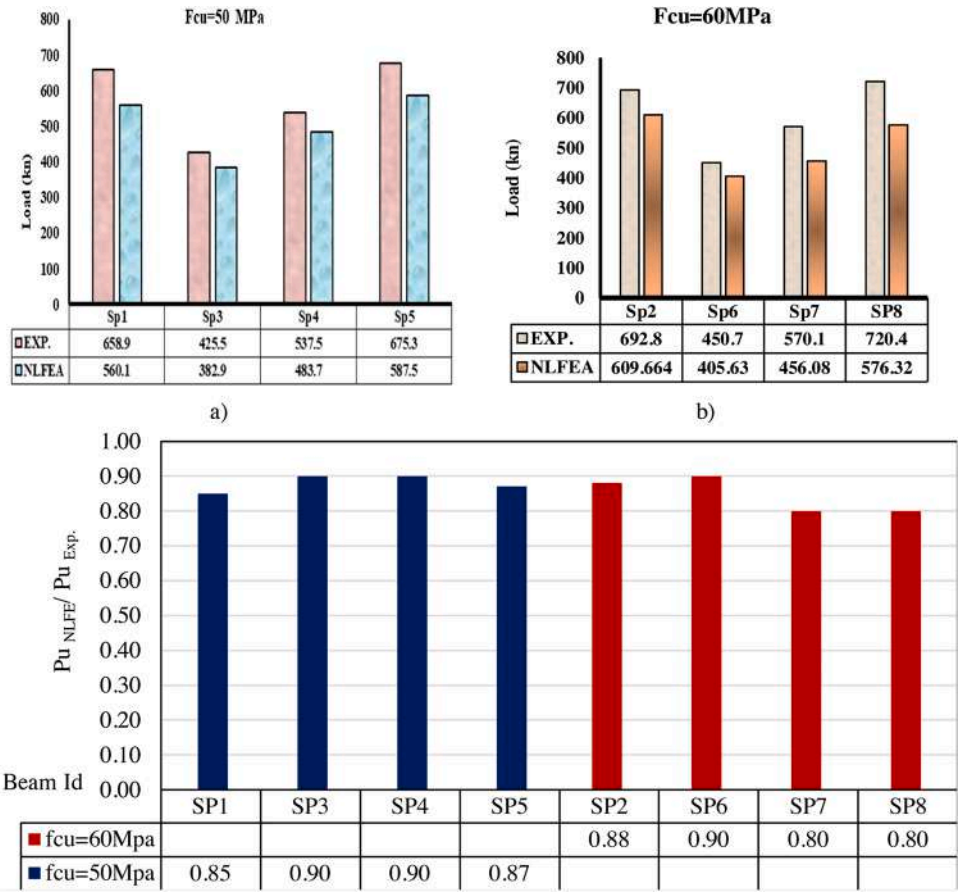

Fig. 16. Comparisons Between Experimental and NLFE; a) Failure Load for f_{cu} = 50MP_a; b) Failure Load for f_{cu} = 60 MP_a, c) Ratio of Pu $_{(NLFE)}$ / Pu $_{(Exp.)}$.

Table 7
Comparisons Between Experimental and NLFEA Results.

Spec. Id.	RFT. Ratio (μ)	f_{cu} (MPa)	Experimental load (kN)		Numerical load (kN)		Δ (mm)		$\frac{Pu\ (NLFE)}{Pu\ (Exp)}$		$\frac{\Delta(NLFE)}{\Delta\ (Exp)}$
			First crack	Max. load	First crack	Max. load	Δ_{exp}	Δ_{NLFE}	First crack	Max. load	
SP1	0.83μ_{bs}	50	170	658.9	9.0	560.1	12.24	10.4	0.52	0.85	0.85
SP3	0.80 μ_b	50	110	425.5	9.0	382.9	5.70	5.13	0.75	0.90	0.90
SP4	1.00 μ_b	50	117	537.5	9.0	483.7	6.58	5.13	0.60	0.90	0.90
SP5	1.20 μ_b	50	120	675.3	9.0	587.5	9.70	6.16	0.50	0.87	0.87
SP2	0.83μ_{bs}	60	175	692.8	11.0	609.7	11.88	8.40	0.57	0.88	0.88
SP6	0.80 μ_b	60	115	450.7	11.0	405.6	9.50	7.83	0.84	0.90	0.90
SP7	1.00 μ_b	60	118	570.1	11.0	456.1	9.30	7.44	0.68	0.80	0.80
SP8	1.20 μ_b	60	130	720.4	11.0	657.3	7.24	7.00	0.58	0.80	0.95
Average									0.630	0.860	0.880
Standard deviation									0.120	0.040	0.041
Coefficient of variance									0.013	0.002	0.002

For the specimens of the second group of beams having a concrete compressive strength of 60 MPa, the theoretical failure loads were 609.7 kN, 405.6 kN, 456.1 kN, and 657.3 kN for SP2, SP6, SP7, and SP8, respectively. Thus, failure load for SP8 exceeded that for SP2 by 8%. The increase in the failure load in the second group with respect to the first one was attributed to the higher concrete compressive strength.

4.6. The NLFE deflection

The theoretically obtained deflections for all the tested specimens is shown in Table 6. For the first group having f_{cu} 50 MP_a, the

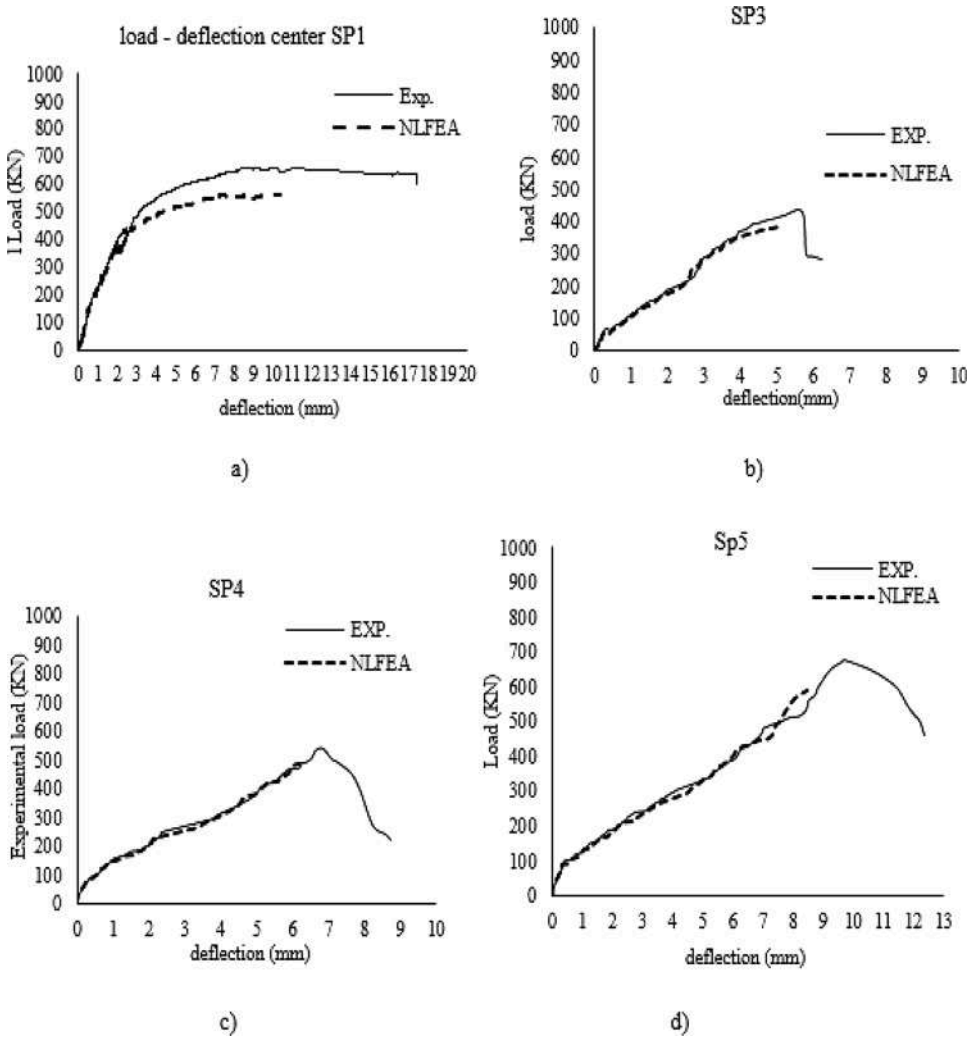

Fig. 17. Comparisons between Experimental and NLFE Failure Load for specimens of f_{cu} = 50 MP_a; a) SP1; b) SP3, c) SP4, d) SP5.

deflection recorded a significant decrease due to using GFRP bars with respect to SP1 reinforced using steel bars. The deflection of the control specimen SP1 recorded 10.4 mm at failure load but it recorded a decrease varying between 40.0%–50.0% for SP3, SP4, and SP5. This indicates the beneficial effect of using GFRP bars in decreasing the deflections of beams.

For the second group, the deflection recorded a value of 8.4 mm for the control specimen SP2 and values of 7.83 mm, 7.44 mm, and 5.80 mm for SP6, SP7, and SP8, respectively. The decrease was apparent in specimen SP8 which was reinforced using 1.2 μ_b as it recorded a decrease of 31.0 %. This indicates the beneficial effect of GFRP bars in decreasing the deflections especially when using ratios exceeding μ_b and high strength concrete.

4.7. Crack pattern and mode of failure

For the crack patterns of the two control beams having compressive strengths of concrete equal to 50 MPa or 60 MPa, the crack pattern is featured with cracks propagating in the tension zone as shown in Fig.13. The failure mode was tension failure T.F.

The behavior of SP3 was like that of SP6 having the same reinforcement ratio equal to 0.8 μb. The concrete was still able to carry the load, but sudden rupture occurred in the GFRP. Thus, these two beams were characterized by GFRP rupture failure (R.F) in the bars. For this reinforcement ratio, the failure mode of the first group was the same as the second group in both the cracks propagation and mode of failure.

5. Comparisons between experimental and NLFEA results

A good agreement was obtained between the experimental and the NLFE results by applying the model using ANSYS-2019-R1. The comparisons were carried out for the failure loads, deflections, the first crack loads and the crack patterns.

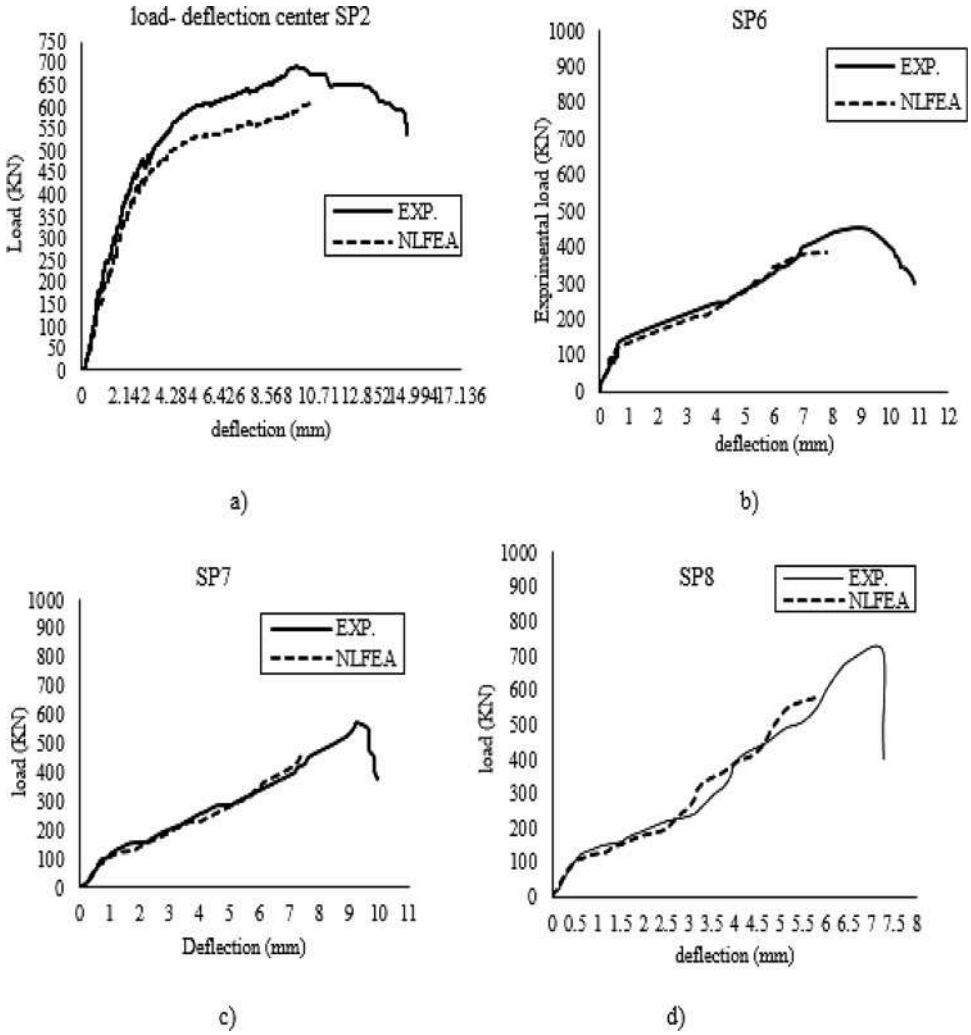

Fig. 18. Comparisons Between Experimental and NLFE Failure Load for specimens of f_{cu} = 60 MP_a; a) SP2; b) SP6, c) SP7, d) SP8.

5.1. *Comparison between experimental and NLFE crack patterns and modes of failure*

By making a comparison between the crack patterns of the control beams having compressive strengths for concrete of 50 MPa or 60 MPa; the crack patterns are featured with cracks propagation in the tension zone for both the experimental and numerical patterns. Fig. 14a shows the tension failure T.F in both beams.

Specimens, SP5 and SP8 which have the same reinforcement area of **1.2 μ_b** GFRP ratio in tension, indicated high ultimate load, low deflection, and a decrease in the number of tension cracks with less propagation as obtained from the experimental patterns as shown in Fig. 15a. The cracks patterns show a good agreement between the NLFEA results and the experimental ones.

5.2. *Comparison between experimental and NLFE failure loads*

Fig. 16 showed a good agreement between the experimental & NLFEA load capacity. Pu NLFEA/Pu exp.

Table 7 shows a comparison between the experimental & NLFEA results. For group I have a concrete strength of 50 MP_a, the Pu NLFEA/Pu exp ratio had an average ratio of 0.88. For group II, with concrete strength 60 MP_a, the ratios were 0.88, 0.90, 0.80 and 0.80 for SP2, SP6, SP7, and SP8 respectively. Finally, for both groups I and II, the average ratio of the agreement for all specimens is 0.86 with a standard deviation of 0.04. Thus, the comparisons in Table 7 show that the results of the developed NLFE model are in excellent correlation with the behavior of the tested specimens and correctly predicted their behavior.

5.3. *Comparison between experimental and NLFE deflections*

Figs. 17 and 18 show comparisons between both the experimental and NLFEA deflections at the maximum failure loads. Fig. 19

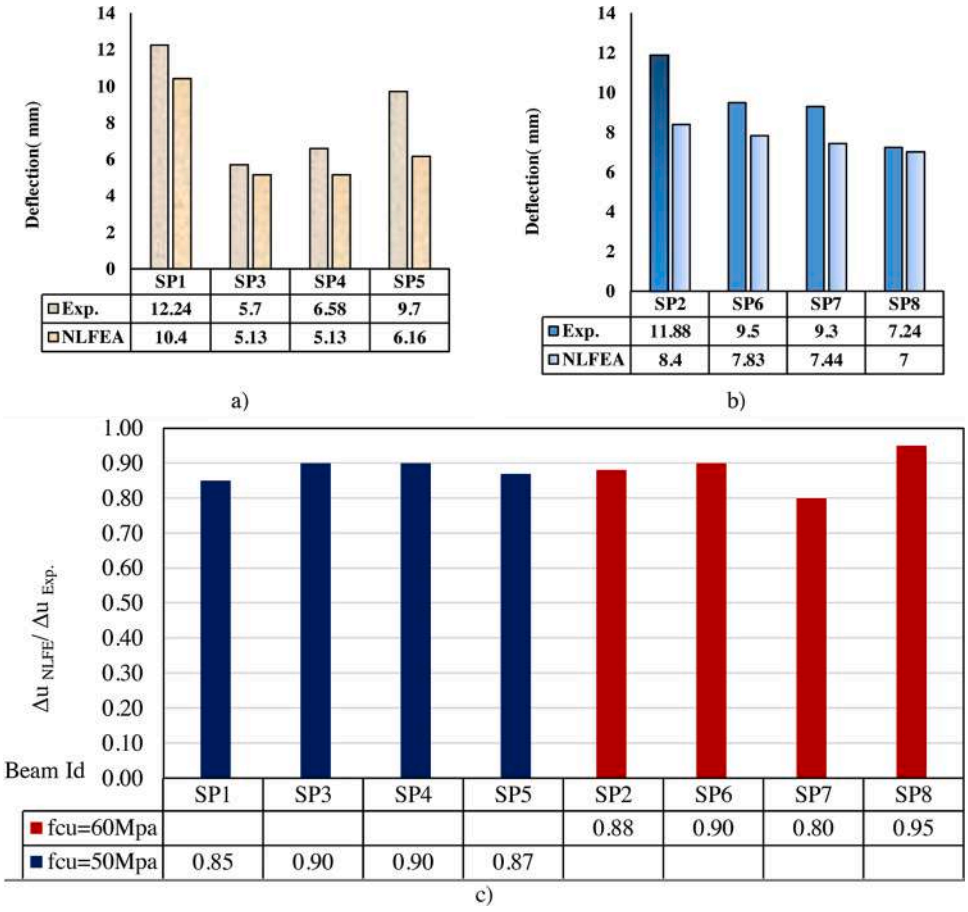

Fig. 19. Comparisons between Experimental and NLFE; a) Deflections for f_{cu} = 50MP_a; b) Deflections for f_{cu} = 60 MP_a, c) Ratio of Δu ($_{NLFE}$) / Δu ($_{Exp.}$).

shows the obtained deflections for all groups I and II for both the experimental and numerical studies.

Table 7 shows a deflection ratio $\Delta_{u\ NLFEA}$ / $\Delta_{u\ exp}$. For the control specimen SP1 of 0.85, and values of 0.90, 0.90 and 0.87 for SP3, SP4 and SP5. For the second group the ratios were 0.88, 0.90, 0.80 and 0.95 for SP2, SP6, SP7, and SP8 respectively with an average ratio of agreement of 0.88.

The load-deflection curves for all the tested specimens and numerical results showed a good agreement of an average of 88.0 %. This indicates that the numerical models provided an acceptable load-deflection response as in Table 7.

6. Conclusions

This study investigated the flexural behavior of concrete deep beams reinforced with locally produced glass fiber reinforced polymer (GFRP) bars. Within the scope of this investigation and considering the materials used; and the comparison of the experimental and the numerical model results, derived in this study, the following conclusions could be made:

1 The locally produced GFRP bars exhibit reasonable mechanical properties compared with commercial products in terms of tensile strength. The recorded tensile strength was (650 MPa, 740 MPa and 1075 MPa) for diameters of (8.0 mm, 10.0 mm, and 12.0 mm) respectively.
2 Beam SP5, reinforced with 1.2 $\boldsymbol{\mu_b}$ showed a decrease of about 20 % in deflection compared with beam SP1 reinforced with steel bars.
3 Increasing the concrete strength in beams reinforced with 1.2 $\boldsymbol{\mu_b}$ led to a decrease in deflection of about 39 % in case of SP8 compared with SP2. Thus, increasing the concrete strength of deep beams has a significant effect in decreasing the deflection when using GFRP reinforcement.
4 For the same compressive strength, the use of GFRP reinforcement bars instead of steel bars had a slight effect on increasing the failure loads of the beams. This increase in the failure load reached 4% in case of beam SP8 reinforced with 1.2 $\boldsymbol{\mu_b}$ compared with SP2 reinforced with steel.

5 For SP4, the recorded GFRP strain was 0.01 and the recorded concrete strain was 0.005, exceeding the ultimate values. Thus, rupture of the GFRP bars took place accompanied with concrete compression strut failure.
6 The analysis adequately reflected the trend of the experimental results. At the ultimate level, the overall average ratio $Pu_{NLFE.}$ / Pu_{EXP} was 86 %. A good agreement between experimental & numerical results showed of an average of 88.0 %.

Declaration of Competing Interest

We declare that they are no known competing financial interests or personal relationships that could have appeared to influence the work reported in this paper.

References

[1] H.V. GangaRao, Design of concrete members reinforced with GFRP bars, Proceedings of the Third International Symposium on Non-Metallic (FRP) Reinforcement for Concrete Structures (1997) 143–150.
[2] F.G. Kong, Reinforced Concrete Deep Beams, 2nd ed., 2003. Taylor & Francis, pp.2.
[3] K.H. Tan, N. Zhang, Size effect in RC deep beams experimental investigation and STM verification, Eng. Struct. 29 (2007) 3241–3254.
[4] M. Habeeb, A. A, Flexural behavior of continuous GFRP reinforced concrete beams, J. Compos Constr. 12 (2) (2008) 115–124.
[5] G. Campione, Flexural behavior of steel fibrous reinforced concrete deep beams, ASCE J. Structural Eng. 138 (2) (2012) 235–246, 2012.
[6] H.Q. Majeed, Nonlinear finite element analysis of steel fiber reinforced concrete deep beams with and without opening, J. Eng. Dev. 18 (2) (2012).
[7] Dipti R. Sahoo, Carlos A. Flores, Shih– Ho Chao, Behavior of steel Fiber – reinforced concrete deep beams with large opening, ACI Struct. J. 109 (2) (2012).
[8] A.M. Erfan, H.E. Hassan, K.M. Hatab, T.A. El-Sayed, The flexural behavior of nano concrete and high strength concrete using GFRP, Constr. Build. Mater. 247 (2020) 118664.
[9] ACI Committee 318, Building Code Requirements for Reinforced Concrete (ACI 318-14) and Commentary (ACI 318R-14), American Concrete Institute, Farmington Hills, Mich, 2014.
[10] Doo-Yeol Yoo, Nemkumar Banthia, Young-Soo Yoon, Flexural behavior of ultra-high-performance fiber-reinforced concrete beams reinforced with GFRP and steel rebars, Eng. Structure 111 (2016) 246–262.
[11] A. Wolanski, Flexural Behavior of Reinforced and Prestressed Concrete Beams Using Finite Element Analysis". Master Thesis, Marquette University, Milwaukee, Wisconsin, 2004.
[12] R.H. Shah, S.V. Mishra, Crack deformation characteristics of SFRC deep beams" IE (I), J. Geogr. Inst. Jovan Cviji? Sasa 31 (July) (2004).
[13] ACI, Guide Test Methods for fiber-reinforced Polymers (FRPs) for Reinforcing or Strengthening Concrete Structures. ACI Committee, 2004.
[14] Keun–Hyeok Yang, Hee–Chang Eun, Heon–Soo Chung, The influence of web openings on the structural behavior of reinforced high – strength concrete deep beams, Eng. Struct. (2006) 1825–1834.
[15] K.H. Tan, N. Zhang, Size effect in RC deep beams experimental investigation and STM verification, Eng. Struct 29 (2007) 3241–3254.
[16] Juan De Dios, slubell Adam, Behavior of Concrete Deep Beam with High Strength Reinforcement. Structural Engineering Report no. 277, 2008.
[17] D. Kuchma, S. Yindeesuk, T. Nagle, J. Hart, H.H. Lee, Experimental validation of strut – and – tie method for complex regions, ACI Struct. J. 105 (5) (2008) 578–589.
[18] V. Vengatachalapathy, R. Ilangovan, A study on steel Fiber reinforced concrete deep beams with and without openings, Int. J. Civ. Struct. Eng. 1 (3) (2010) 509–517.
[19] M. Mohammadhassani, M.Z. Jumaat, A. Ashour, M.An. Jameel, Failure modes and serviceability of high strength self-compacting concrete deep beams, Eng. Fail. Anal. 18 (2011), pp. 2272-228.
[20] ECP 208, Egyptian Code of Practice for Design Principles of the Use of Fiber Reinforced Polymers in Construction. Permanent Committee, 2018.
[21] T. Xie, M.S. Mohamed Ali, P. Vistinin, D.J. Oehlers, Partial interaction model of flexural behavior of PVA Fiber–Reinforced concrete beams with GFRP bars, J. Compos. Constr. 22 (5) (2018).
[22] Ahmed Sabry Farghaly, Brahim Benmokrane, Shear Behavior of FRP-Reinforced Concrete Deep Beams without Web Reinforcement, ASCE, 2013.
[23] A.M. Erfan, R.M. Abd Elnaby, A.A. Badr, T.A. El-sayed, Flexural behavior of HSC one way slabs reinforced with basalt FRP bars, Case Stud. Constr. Mater. 14 (2021) e00513.
[24] Constantin E. Chalioris, K. Parthena-Maria, A. Kosmidou Iand Nikos, Papadopoulos, Investigation of a new strengthening technique for RC deep beams using carbon FRP ropes as transverse reinforcements, Fibers "MDPI (July) (2018).
[25] Chris G. Karayannis, Parthena-Maria K. Kosmidou, E. Constantin, Reinforced concrete beams with carbon-fiber-Reinforced polymer bars—experimental study, Fibers "MDPI" (December) (2018).
[26] Parthena-Maria K. Kosmidou, Constantin E. Chalioris, Chris G. Karayannis, Flexural/Shear strength of RC beams with longitudinal frp bars an analytical approach, Comput. Concrete J. 22 (6 Decmber) (2018).
[27] Constantin E. Chalioris, Adamantis G. Zapris, Chris G. Karayannis, U-Jacketing Applications of Fiber-reinforced Polymers in Reinforced Concrete T-Beams against Shear—Tests and Design", Fibers "MDPI, 17 February, 2020.
[28] T.A. El-Sayed, A. Erfan, Improving shear strength of beams using ferrocement composites, Constr. Build. Mater. 172 (2018) 608–617.
[29] Yasir M. Saeed, Wisam A. Aules, Franz N. Rad, Anis M. Raad, Tensile behavior of FRP anchors made from CFRP ropes epoxy-bonded to uncracked concrete for flexural strengthening of RC columns, Case Stud. Constr. Mater. 13 (September) (2020).
[30] T.A. El-Sayed, Flexural behavior of RC beams containing recycled industrial wastes as steel fibers, Constr. Build. Mater. 212 (2019) 27–38.
[31] T.A. El-Sayed, Y.B. Shaheen, Flexural performance of recycled wheat straw ash-based geopolymer RC beams and containing recycled steel fiber, December, Structures 28 (2020) 1713–1728.
[32] A.M. Ibrahim, A. Erfan, Finite element modeling of reinforced concrete beams with openings, Jokull J. 67 (9) (2017) 16–32.
[33] A.M. Erfan, Y.A. Algash, T.A. El-Sayed, Experimental & Analytical Flexural Behavior of Concrete Beams Reinforced with Basalt Fiber reinforced Polymers Bars, 2019.
[34] A.M. Erfan, Y.A. Algashb, T.A. El-Sayed, Experimental and Analytical Behavior of HSC Columns Reinforced with Basalt FRP Bars, 2019.
[35] T.A. El-Sayed, A.M. Erfan, R.M. Abd El-Naby, Flexural behavior of RC beams by using agricultural waste as a cement reinforcement materials, J. Eng. Res. Rep. (2019) 1–12.
[36] T.A. El-Sayed, Y.A. Algash, Flexural behavior of ultra-high performance geopolymer RC beams reinforced with GFRP bars, Case Stud. Constr. Mater. (2021) e00604.
[37] Egyptian Standards Specification, E.S.S, 4756-11, Physical and Mechanical Properties Examination of Cement, Part 1, Cairo, 2012.
[38] ANSYS, "Engineering Analysis system user's Manual" 201, vol. 1&2, and theoretical manual. Revision 8.0, Swanson analysis system inc., Houston, Pennsylvania.